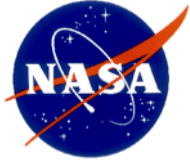# Combinations of Earth Orientation Measurements: SPACE2018, COMB2018, and POLE2018

J.T. Ratcliff and R.S. Gross

ABSTRACT

Independent Earth orientation measurements taken by the space-geodetic techniques of lunar and satellite laser ranging, very long baseline interferometry, and the Global Positioning System have been combined using a Kalman filter. The resulting combined Earth orientation series, SPACE2018, consists of values and uncertainties for Universal Time, polar motion, and their rates that span from September 28, 1976, to June 28, 2019, at daily intervals and is available in versions with epochs given at either midnight or noon. The space-geodetic measurements used to generate SPACE2018 have then been combined with optical astrometric measurements to form two additional combined Earth orientation series: (1) COMB2018, consisting of values and uncertainties for Universal Time, polar motion, and their rates that span from January 20, 1962, to June 28, 2019, at daily intervals and which are also available in versions with epochs given at either midnight or noon; and (2) POLE2018, consisting of values and uncertainties for polar motion and its rate that span from January 20, 1900, to June 22, 2019, at 30.4375-day intervals.

ACKNOWLEDGMENTS

TABLE OF CONTENTS

INTRODUCTION

Reference series of Earth orientation parameters (EOP) obtained by combining independent measurements of Earth's orientation are generated annually at the Jet Propulsion Laboratory (JPL) in support of tracking and navigation of interplanetary spacecraft. This report describes the generation of the most recent such combined Earth orientation series: SPACE2018, COMB2018, and POLE2018. Since the procedures used to generate these most recent series are similar to those used to generate previous such combinations, only a brief description of their generation is given here. Further details regarding the approach used at JPL to annually combine independent measurements of Earth's orientation can be found in Gross (1996, 2000) and Gross et al. (1998)

SPACE2018

Data Sets Combined to Form SPACE2018

SPACE2018 is a combination of independent space-geodetic measurements of Earth's orientation. Table 1 lists the space-geodetic series used in generating SPACE2018, giving their identifiers, the number of measurements from each series that were actually incorporated into SPACE2018, and the time interval spanned by those measurements. Note that the University of Texas Center for Space Research (UTCSR) satellite laser ranging (SLR) Universal Time (UT) values were not used in generating SPACE2018 due to problems associated with separating this component of Earth's orientation from the effects of unmodeled forces acting on the satellite that cause the node of its orbit to drift (see Gross et al. 1998, p. 217 for further discussion about this point). For similar reasons, the International Laser Ranging Service (ILRS) satellite laser ranging length-of-day (LOD) values have not been used in generating SPACE2018.

Since it was desirable to combine only independent measurements of Earth's orientation, only those series listed in Table 1 were used, even though other space-geodetic series are available from other analysis centers. When more than one series determined by the same measurement technique was used, care was taken to ensure that the measurements themselves were not included more than once. In particular, polar motion measurements from the JPL Global Positioning System (GPS) series were only used until the start of the International Global Navigation Satellite Systems (GNSS) Service (IGS) combined series EOP(IGS) 95 P 01 on January 1, 1995; polar motion measurements from the IGS combined EOP(IGS) 95 P 01 were then used until the start of the IGS combined series EOP(IGS) 95 P 02 on June 30, 1996; polar motion measurements from the IGS combined series EOP(IGS) 95 P 02 were then used until the start of the accumulated IGS Solution Independent Exchange (SINEX) combined series EOP(IGS) 00 P 03 on February 26, 2000; and polar motion measurements from the accumulated IGS SINEX combined series EOP(IGS) 00 P 03 were used thereafter. Similarly, LOD measurements from the IGS combined series EOP(IGS) 95 P 02 were used until it ended on February 25, 2000 with LOD measurements from the accumulated IGS SINEX combined series EOP(IGS) 00 P 03 used thereafter. In addition, UT measurements from the National Oceanic and Atmospheric Administration (NOAA) International Radio Interferometric Surveying (IRIS) Intensive UT1 series were used until it ended on December 31, 1994; measurements from the United States Naval Observatory (USNO) National Earth Orientation Service (NEOS) Intensive UT1 series were then used until it ended on December 4, 2000; and measurements from the Goddard Spaceflight Center (GSFC) NEOS Intensive UT1 series were used thereafter. Finally, polar motion measurements from the UTCSR SLR series EOP(CSR) 96 L 01 were used until it ended on February 3, 1996, with measurements from the ILRS combined SLR series being used thereafter.

Data Preprocessing and Treatment of Tide-Induced Rotational Variations

The Earth orientation series listed in Table 1 were preprocessed by removing leap seconds from the Universal Time (UT1) values and, when necessary, by correcting the UT1 values to be consistent with the extended definition of Greenwich Sidereal Time (GST) as adopted by the International Earth Rotation and Reference Systems Service (IERS; IERS 1997, p. I49). Since most of the series listed in Table 1 were already consistent with the extended definition of GST, this correction needed to be applied to only the NOAA IRIS Intensive UT1 series.

Table 1. Data Sets Combined to Form SPACE2018*

Data Set Name	Data Type	Analysis Center	Reference	Data Span	Number
LLR (JPL19M01; VOL, UT0)					
McDonald Cluster	LLR	JPL	Williams et al. (2012)	Oct. 5, 1976, to Oct. 13, 2013	895
OCA	LLR	JPL	Williams et al. (2012)	Apr. 7, 1984, to Jun. 28, 2019	2269
Haleakala	LLR	JPL	Williams et al. (2012)	Nov. 14, 1984, to Aug. 29, 1990	110
Apache Point	LLR	JPL	Williams et al. (2012)	Jun. 4, 2006, to Oct. 15, 2016	680
Crimea	LLR	JPL	Yagudina et al. (2018)	Aug. 9, 1982, to Oct. 29, 1983	13
UTCSR (CSR96L01)					
LAGEOS Polar Motion	SLR	UTCSR	Eanes & Watkins (1996)	Sep. 27, 1976, to Feb. 4, 1996	2218
ILRSA (17Jul19; Polar motion)					
ILRS Primary Combination	SLR	ASI-CGS	Sciaretta et al. (2010)	Feb. 5, 1996, to Jun. 28, 2019	8493
DSN (JPL97R01; T, V)					
California-Spain Cluster	VLBI	JPL	Steppe et al. (1997)	Nov. 26, 1979, to Jun. 23, 2019	1279
California-Australia Cluster	VLBI	JPL	Steppe et al. (1997)	Oct. 28, 1978, to Sep. 30, 1997	698
NOAA (NOAA95R02)					
IRIS Intensive UT1	VLBI	NOAA	Ray et al. (1995)	Apr. 2, 1984, to Dec. 31, 1994	2392
USNO (N9903)					
NEOS Intensive UT1	VLBI	USNO	Eubanks et al. (1999)	Jan. 4, 1995, to Dec. 4, 2000	1497
NASA/GSFC (GSF2016a)					
NEOS Intensive UT1	VLBI	GSFC	NASA/GSFC, VLBI Group (2018)	Dec. 6, 2000, to Jun. 28, 2019	6133
NASA/GSFC (GSF2016a)					
Multibaseline	VLBI	GSFC	NASA/GSFC, VLBI Group (2018)	Apr. 12, 1980, to Jun. 28, 2019	5622
NASA/GSFC (GSFC1122)					
Westfort-Fort Davis	VLBI	GSFC	Gordon et al. (1999)	Jun. 25, 1981, to Jan. 1, 1984	105
Westfort-Mojave	VLBI	GSFC	Gordon et al. (1999)	Mar. 21, 1985, to Aug. 6, 1990	18
GPS (21APR04; Polar motion)					
Post-processed Flinn Analysis	GPS	JPL	Heflin et al. (2004)	Jun. 10, 1992, to Dec. 31, 1994	817
GPS (IGS95P01; Polar motion)					
IGS Final Combined	GPS	NRCan	Kouba & Mireault (1997)	Jan. 1, 1995, to Jun. 29, 1996	546
GPS (IGS95P02; Polar motion)					
IGS Final Combined	GPS	CODE	Mireault & Kouba (2000)	Jun. 30, 1996, to Feb. 26, 2000	1337
GPS (IGS00P03; Polar motion)					
IGS SINEX Combined	GPS	IGN	Rebischung & Garayt (2013)	Feb. 27, 2000, to Jun. 28, 2019	7051
GPS (IGS95P02; LOD)					
IGS Final Combined	GPS	CODE	Mireault & Kouba (2000)	Feb. 23, 1997, to Feb. 26, 2000	1098
GPS (IGS00P03; LOD)					
IGS SINEX Combined	GPS	IGN	Rebischung & Garayt (2013)	Feb. 27, 2000, to Jun. 28, 2019	7048

* LLR, lunar laser ranging; JPL, Jet Propulsion Laboratory; VOL, variation of latitude; UT, Universal Time; OCA, Observatoire de la Côte d'Azur; UTCSR, University of Texas Center for Space Research; LAGEOS, Laser Geodynamic Satellite; SLR, satellite laser ranging; ILRS, International Laser Ranging Service; ASI, Agenzia Spaziale Italiana; CGS, Centro di Geodesia Spaziale; DSN, Deep Space Network; T, transverse; V, vertical; VLBI, very long baseline interferometry; NOAA, National Oceanic and Atmospheric Administration; IRIS, International Radio Interferometric Surveying; USNO, United States Naval Observatory; NEOS, National Earth Orientation Service; NASA, National Aeronautics and Space Administration; GSFC, Goddard Space Flight Center; GPS, Global Positioning System; IGS, International Global Navigation Satellite System (GNSS) Service; ITRF, International Terrestrial Reference Frame; NRCan, Natural Resources Canada; CODE, Center for Orbit Determination in Europe; IGN, Institut National de l'Information Géographique et Forestière; SINEX, solution independent exchange; LOD, length of day.

3

Table 2. Changes to the IGS Reference Frame.

Date of Change	Previous Frame	New Frame	Reference
June 30, 1996	ITRF93	ITRF94	IGS Analysis Center Coordinator (2012)
March 1, 1998	ITRF94	ITRF96	Kouba et al. (1998)
August 1, 1999	ITRF96	ITRF97	Springer (1999)
February 27, 2000	ITRF97	IGS97	Ferland (2000)
December 2, 2001	IGS97	IGS00	Weber (2001)
January 11, 2004	IGS00	IGb00	Ferland (2003)
November 5, 2006	IGb00	IGS05	Ferland (2006)
April 17, 2011	IGS05	IGS08	Rebischung et al. (2011, 2012)
October 7, 2012	IGS08	IGb08	Rebischung (2012)
January 29, 2017	IGb08	IGS14	Rebischung (2016)

Rotational variations caused by solid-Earth and ocean tides were also removed from the UT1 values. The effect of the solid-Earth tides was removed by using the model of Yoder et al. (1981); the model of Kantha et al. (1998) was used to remove the effect upon UT1 of the ocean tides at the Mf, Mf′, and Mm tidal frequencies. Since the Yoder et al. (1981) model already includes a contribution from the equilibrium ocean tides, only the Kantha et al. (1998) oceanic corrections to the Yoder et al. (1981) model were actually removed. Also note that the Kantha et al. (1998) model was used to remove the effect of ocean tides on only UT1, not on polar motion. Ocean-tide-induced polar motion variations were not removed from any of the polar motion observations. Finally, the only Earth orientation series listed in Table 1 that includes the effects of semidiurnal and diurnal ocean tides on the Earth's orientation is the NOAA IRIS Intensive UT1 series. This series included these effects by adding to the released UT1 values the model of Herring (1993, also see Herring & Dong 1994). Hence, the same Herring (1993) model was used to remove them.

From time to time, the IGS has changed the terrestrial reference frame used to express its products, usually related to updates of the International Terrestrial Reference Frame (ITRF). A chronology of the relevant IGS changes is given in Table 2. Such changes in reference frame potentially introduce discontinuities into the IGS combined Earth orientation series. However, the IGS Final combined series EOP(IGS) 95 P 02 and the accumulated IGS SINEX combined series EOP(IGS) 00 P 03 used here have had each of these segments aligned to the same IGS reference frame. Thus, to within the uncertainty in determining the corrections required to align each segment, the IGS combined series EOP(IGS) 95 P 02 and EOP(IGS) 00 P 03 used here should be reasonably consistent with each other. They were, therefore, concatenated with one common set of bias-rate corrections being determined for them, as described below.

Adjustments Made to Space-Geodetic Series Prior to Combination

Prior to combining the series listed in Table 1 to form SPACE2018, series-specific corrections were applied for bias and rate, the stated uncertainties of the measurements were adjusted by multiplying them by series-specific scale factors, and outlying data points were deleted. Values for the bias-rate corrections and uncertainty scale factors were determined by an iterative procedure wherein each series was compared, in turn, to a combination of all others. In order to minimize interpolation error (see Gross et al., 1998, pp. 223–225), the comparison of each series to its reference combination was done at the epochs of the measurements of that series by generating its reference combination using a

Kalman filter that interpolates to (and prints its EOP estimates at) the exact epochs of those measurements. Also, both the bias-rate corrections and the uncertainty scale factors for all components of a given series were determined simultaneously in a multivariate approach using nonlinear weighted least squares. Using a multivariate approach allows the correlations between the components to be taken into account when determining the bias-rate corrections and uncertainty scale factors (see Gross et al., 1998, pp. 22).

All of the series listed in Table 1, except for the Westford–Mojave and Westford–Fort Davis baselines of GSFC VLBI and LLR from the Crimea station, were included in the iterative procedure. Details of the iterative procedure are described in Gross (1996, 2000) and Gross et al. (1998) and will not be repeated here. These details include:

1. Use of a reference series, SPACE2017 (Ratcliff & Gross, 2018), for initial bias-rate alignment;

2. Analysis of each data type in its natural reference frame;

3. Clustering of the McDonald LLR stations and, separately, the DSN very long baseline interferometry (VLBI) stations in California, Australia, and Spain;

4. Initial convergence on values for the series-specific bias-rate corrections and uncertainty scale factors prior to the start of outlier detection and deletion; and

5. Final convergence on these values after detecting and deleting all data outliers.

At the end of the iterative procedure, relative bias-rate corrections have been determined that make the series agree with each other in bias and rate; uncertainty scale factors have been determined that make the residual of each series have a reduced chi-square near one when differenced with a combination of all others; and outlying data points (those with residual values greater than four times their adjusted uncertainties) have been deleted. A total of 175 data points, or about 0.34% of those combined, were thus deleted.

For GSFC NEOS Intensive and GSFC Multibaseline VLBI, the initial alignment to SPACE2017 was performed individually for each baseline containing at least 90 data points and spanning more than 1 year. Baselines containing less than 1 year of data, or fewer than 90 data points, or for which a reliable covariance adjustment could not be obtained were aligned as a group to SPACE2017. Subsequent steps of the iterative procedure were then conducted independently on the individual baseline groups.

Starting April 17, 2011 the IGS changed their procedure for estimating uncertainty in GPS EOP values. This introduced a change in magnitude of the polar motion X (PMX), polar motion Y (PMY), and LOD uncertainties of approximately a factor of 6. To account for this sudden change, uncertainty scale factor values after April 17, 2011 were estimated separately from those of earlier epochs using a trial reference series. These trial scale factors were applied to the original IGS GPS data, which were then used in the iterative procedure described above to form a final reference series. The resulting scale factors shown in Table 3 for the IGS00P03 data set include the contribution of both the trial scale factors and the overall iteratively determined scale factor.

Since the GSFC VLBI data from the Westford–Mojave and Westford–Fort Davis baselines and the LLR data from the Crimea station contain relatively few measurements over a short time span, they were not included in the iterative procedure. Instead, relative bias-rate corrections for these series were determined that make them agree in bias and rate with an intermediate combination that

Table 3. Adjustments to Space-Geodetic Series[a]

Data Set Name	Bias, mas			Rate, mas/yr			Uncertainty Scale Factor		
LLR (JPL18M01)	VOL	UT0		VOL	UT0		VOL	UT0	
McDonald Cluster	−0.0045 ± 0.0727	−0.0065 ± 0.0756		0.0269 ± 0.0154	0.0156 ± 0.0146		1.3895	1.3019	
OCA	0.0432 ± 0.0246	−0.0131 ± 0.0217		−0.0031 ± 0.0012	0.0007 ± 0.0011		1.9062	1.5291	
Haleakala	−2.1660 ± 1.0090	−1.0122 ± 0.6627		−0.3553 ± 0.1932	−0.1528 ± 0.1356		2.4344	2.4048	
Apache Point	−0.0849 ± 0.1130	0.1164 ± 0.1275		0.0051 ± 0.0059	−0.0079 ± 0.0065		1.6286	1.6463	
Crimea	5.3019 ± 57.731	4.7481 ± 85.910		− 0.0001	− 0.0003		1.0622	0.9360	
DSN (JPL97R01)	T	V		T	V		T	V	
California–Australia Cluster	0.5793 ± 0.0184	0.3998 ± 0.0529		0.0764 ± 0.0076	0.0467 ± 0.0237		1.4292	1.1659	
California–Spain Cluster	−0.7214 ± 0.0228	−0.4100 ± 0.0556		0.1017 ± 0.0012	0.0094 ± 0.0033		2.1615	1.4773	
NASA GSFC (1122)	T	V		T	V		T	V	
Westford–Fort Davis	11.3225 ± 3.7992	6.0585 ± 5.8836		1.0375 ± 0.3814	0.6061 ± 0.5885		1.3443	0.9184	
Westford–Mojave	0.7136 ± 1.1025	− 0.4408 ± 1.6912		− 0.0005	− 0.0014		2.5138	0.7283	
GSFC (GSF2016a)[b]	PMX	PMY	UT1	PMX	PMY	UT1	PMX	PMY	UT1
G3GcKuRi	0.2669 ± 0.1016	− 0.1375 ± 0.1038	0.2035 ± 0.1666	0.1302 ± 0.0610	− 0.0622 ± 0.0639	− 0.1268 ± 0.0999	1.3675	1.3908	1.9345
HrRiWfWz	0.5394 ± 0.1693	− 0.6470 ± 0.1767	0.3144 ± 0.2803	0.0573 ± 0.0289	− 0.0677 ± 0.0298	− 0.0010 ± 0.0477	1.1724	1.2437	1.7413
Other Networks	0.0389 ± 0.0049	− 0.1729 ± 0.0044	0.2591 ± 0.0085	− 0.0029 ± 0.0003	0.0033 ± 0.0003	− 0.0082 ± 0.0005	1.7275	1.7282	1.8213
NOAA (95R02)	PMX	PMY	UT1	PMX	PMY	UT1	PMX	PMY	UT1
IRIS Intensive	-----	-----	0.2129 ± 0.0227	-----	-----	0.0480 ± 0.0068	-----	-----	1.0174
USNO (N9903)	PMX	PMY	UT1	PMX	PMY	UT1	PMX	PMY	UT1
NEOS Intensive	-----	-----	− 0.0994 ± 0.0397	-----	-----	0.0405 ± 0.0073	-----	-----	1.3670
GSFC (GSF2016a)[b]	PMX	PMY	UT1	PMX	PMY	UT1	PMX	PMY	UT1
KkNy	-----	-----	0.2551 ± 0.3774	-----	-----	− 0.0092 ± 0.0194	-----	-----	1.2564
KkSvWz	-----	-----	0.3782 ± 0.0953	-----	-----	− 0.0159 ± 0.0049	-----	-----	1.8691
IsWz	-----	-----	− 1.9227 ± 0.6738	-----	-----	0.0776 ± 0.0271	-----	-----	1.6937
NyTsWz	-----	-----	− 0.1154 ± 0.1209	-----	-----	0.0080 ± 0.0064	-----	-----	1.5273
TsWz	-----	-----	− 0.0617 ± 0.0438	-----	-----	0.0060 ± 0.0024	-----	-----	1.7153
KkWz	-----	-----	0.2094 ± 0.0168	-----	-----	− 0.0067 ± 0.0009	-----	-----	1.5324
Other Networks	-----	-----	− 0.0032 ± 0.1309	-----	-----	0.0023 ± 0.0054	-----	-----	2.4811
UTCSR (96L01)	PMX	PMY	UT1	PMX	PMY	UT1	PMX	PMY	UT1
LAGEOS	− 0.2845 ± 0.0102	0.6693 ± 0.0092	-----	0.0419 ± 0.0037	0.1528 ± 0.0034	-----	0.7359	0.7219	-----
ILRSA (17JUL19)	PMX	PMY	LOD	PMX	PMY	LOD	PMX	PMY	LOD
Primary Comb.	0.0553 ± 0.0047	− 0.0735 ± 0.0042	-----	− 0.0052 ± 0.0003	0.0009 ± 0.0003	-----	3.3349	3.1223	-----
GPS (21APR04)	PMX	PMY	LOD	PMX	PMY	LOD	PMX	PMY	LOD
JPL Post-Flinn	− 0.1979 ± 0.0156	0.0875 ± 0.0130	-----	− 0.0179 ± 0.0145	− 0.0246 ± 0.0119	-----	1.2838	0.9165	-----
GPS (IGS95P01)	PMX	PMY	LOD	PMX	PMY	LOD	PMX	PMY	LOD
Final Combined	− 0.1559 ± 0.0552	0.1904 ± 0.0540	-----	0.2214 ± 0.0193	0.3078 ± 0.0190	-----	1.2257	0.9790	-----
GPS (IGS95P02)	PMX	PMY	LOD	PMX	PMY	LOD	PMX	PMY	LOD
Final Combined	0.0542 ± 0.0035	− 0.0193 ± 0.0033	− 0.0054 ± 0.0081	− 0.0029 ± 0.0002	0.0018 ± 0.0002	0.0006 ± 0.0005	1.9906	1.6602	1.7970
GPS (IGS00P03)	PMX	PMY	LOD	PMX	PMY	LOD	PMX	PMY	LOD
before 4/17/2011	0.0542 ± 0.0035	− 0.0193 ± 0.0033	− 0.0054 ± 0.0081	− 0.0029 ± 0.0002	0.0018 ± 0.0002	0.0006 ± 0.0005	1.9906	1.6602	1.7970
after 4/17/2011	0.0542 ± 0.0035	− 0.0193 ± 0.0033	− 0.0054 ± 0.0081	− 0.0029 ± 0.0002	0.0018 ± 0.0002	0.0006 ± 0.0005	14.1797	9.7303	12.8631

a) Reference date for bias-rate adjustment is 1993.0. See Table 1 footnotes. mas, milliarcseconds; PMX, polar motion X; PMY, polar motion Y.
b) GSFC VLBI Station IDs from `ftp://cddis.gsfc.nasa.gov/vlbi/ivscontrol/ns-codes.txt`
G3 = NRAO 85-3; Gc = Gilmore Creek; Hr = HRAS at Fort Davis; Kk = Kokee Park; Ku = 9m at Kokee Park; Mo = 12m at Goldstone; Ny = Ny Alesund, Svalbard, Norway; Ri = Richmond, FL; Sv = Svetloe, Russia; Ts = Tsukuba, Japan; Wf = Westford, MA; Wz = Wettzell, Germany.

was obtained by combining all the other series after applying to them the above iteratively determined bias-rate corrections and uncertainty scale factors. Uncertainty scale factors were determined which make the VLBI and LLR residuals have a reduced chi-square near one when differenced with the intermediate combination. The adjusted VLBI and LLR data were then combined with the iteratively aligned data for subsequent alignment with the ITRF20014 EOPs (described below).

Finally, each series was placed within a particular IERS reference frame by applying to it an additional bias-rate correction that is common to all the series. This additional correction was determined by first combining all the series after applying to them the relative bias-rate corrections and uncertainty scale factors that had been determined for them as described above. This intermediate combination was then compared to the Earth orientation parameters of ITRF2014 (Altamimi

et al., 2016a,b). Only the ITRF2014 EOP values during the interval January 1, 1994 – February 14, 2015 were used for the comparison. Blatantly large outliers in this interval were removed from the ITR2014 series prior to the comparison. The additional bias-rate correction determined from this comparison was then applied to the intermediate combination in order to make it, and therefore each individual series, agree in bias and rate with the ITRF2014 EOP series.

The total bias-rate corrections and uncertainty scale factors determined by the procedures outlined above are given in Table 3. The values of the bias-rate corrections are the sum of: (1) the initial corrections applied to each series to align them to a common reference, (2) all the incremental corrections applied during the iterative procedure, and (3) the additional, common correction applied in order to place each series within that particular reference frame defined by the ITF2014 Earth orientation series (Altamimi et al., 2016b). The values of the uncertainty scale factors are the products of all the incremental scale factors determined during the iterative procedure. The uncertainties of the bias-rate corrections are the 1σ standard errors of the incremental bias-rate corrections determined during the last iteration. There are no bias-rate entries in Table 3 for components that were either not used (e.g., the UTCSR SLR UT1 component) or not available (e.g., the NOAA IRIS Intensive polar motion components). Note that the same common ITRF2014 EOP rate correction is applied to all the data sets, including those such as the Westford–Mojave single baseline VLBI series and Crimea LLR points, for which no relative rate correction could be determined. Therefore, the rate corrections given in Table 3 for those series for which no relative rate corrections could be determined are simply the common ITRF2014 EOP rate correction, but given in the natural reference frame of that series. In these cases, uncertainties for the rate corrections are not given. Also note that the bias-rate corrections in Table 3 for the IGS combined series EOP(IGS) 95 P 02 and EOP(IGS) 00 P 03 are the same. Since these series were initially given within the same IGS reference frame, the series were merged, and a common bias-rate correction was determined for them. However, uncertainty scale factors for these series do differ after April 17, 2011, for the reasons described on page 5.

Combined EOP Series: SPACE2018

A Kalman filter was used to combine the series listed in Table 1 after the bias-rate corrections and uncertainty scale factors listed in Table 3 had been applied to them. The resulting combined Earth orientation series, SPACE2018, consists of values (Figure 1) and 1σ standard errors (Figure 2) for polar motion, Universal Time, and their rates spanning September 28, 1976, to June 28, 2019, at daily intervals; and it is available in versions for which the epochs are given at either midnight or noon. Leap seconds have been restored to UT1, and the effects of the solid Earth and ocean tides have been added back to the UT1 values using the same models for these effects that were originally used to remove them from the raw series: namely, the Yoder et al. (1981) model for the solid Earth tides and the Kantha et al. (1998) model for the ocean tides. However, semidiurnal and diurnal ocean tidal terms have not been added to and are therefore not included in the SPACE2018 UT1 values.

Figure 3 is a plot of the difference between the SPACE2018 polar motion, UT1, and LOD values and those of the ITRF2014 Earth orientation series. Tabulated root-mean-square (rms) differences between SPACE2018 and ITRF2014 EOPs are inset. SPACE2018 is very consistent with ITRF2014 EOPs, especially after January 1, 2000, where the rms of their differences are 0.042 milliarcseconds (mas) in the x-component of polar motion, 0.037 mas in the y-component, 0.088 milliseconds (ms) in UT1, and 0.069 ms in LOD. Prior to 2000, the differences exhibit greater variability. The blatant outliers that were removed from the ITRF2014 EOP series when determining the bias-rate corrections

have been retained for this comparison and can be seen in panel (c) near the years 1996 and 2000. These outliers are included in the computation of rms values. SPACE2018 is also very consistent with IERS Bulletin A (Stamatakos et al., 2015) as shown in Figure 4 where rms differences after January 1, 2000 are 0.047 mas in the x-component, 0.037 mas in the y-component, 0.013 ms in UT1, and 0.013 ms in LOD.

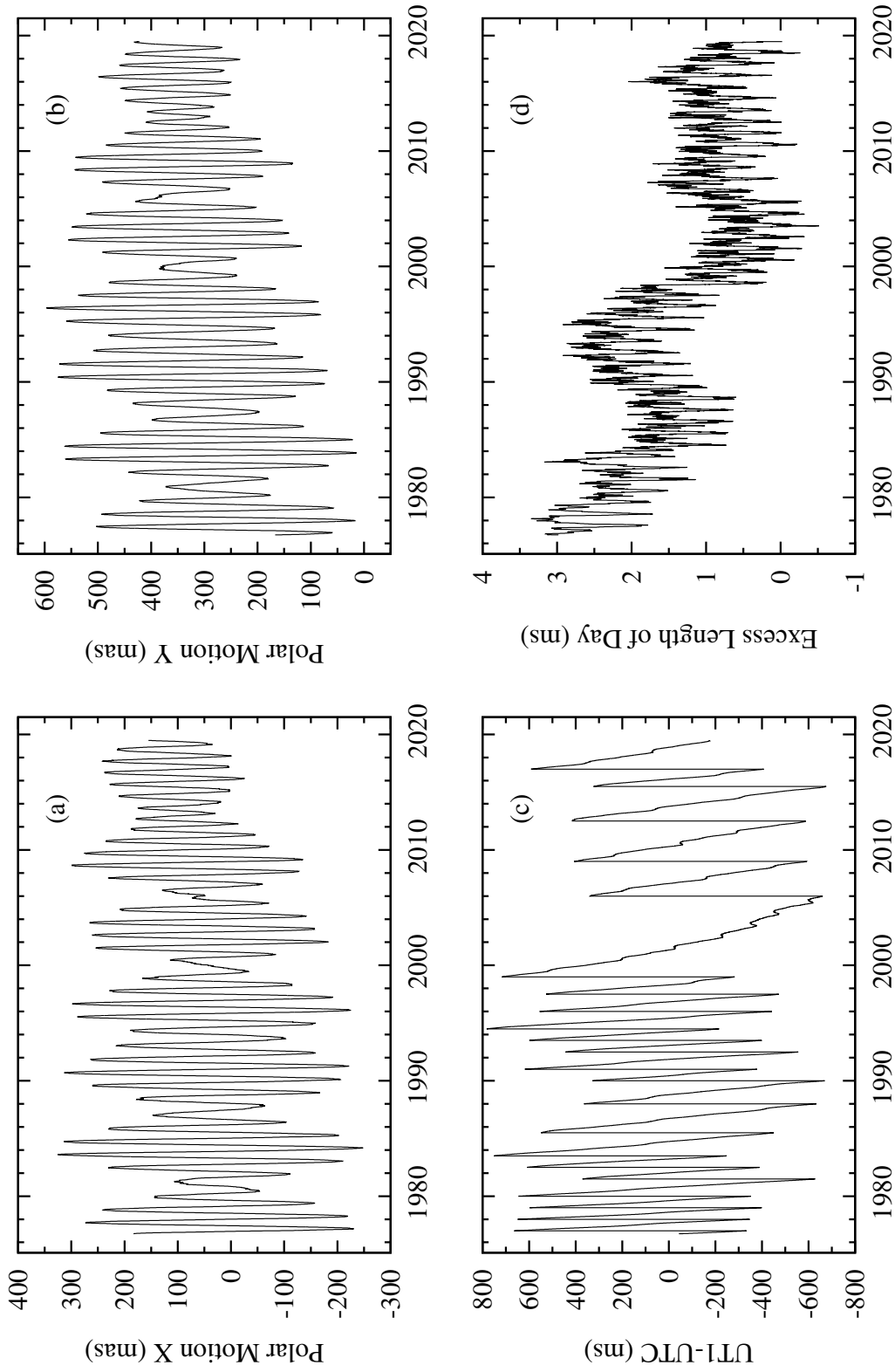# A Combined Earth Orientation Series: SPACE2018

Figure 1. Plots of the x-component of polar motion (1a), y-component of polar motion (1b), UT1–UTC (1c), and excess length-of-day (1d) as given by the combined Earth orientation series SPACE2018. The discontinuous changes in the plot of UT1–UTC are caused by the presence of leap seconds. Note that the UT1–UTC values displayed in (1c) include the tidal variations, whereas the excess length-of-day values shown in (1d) do not.

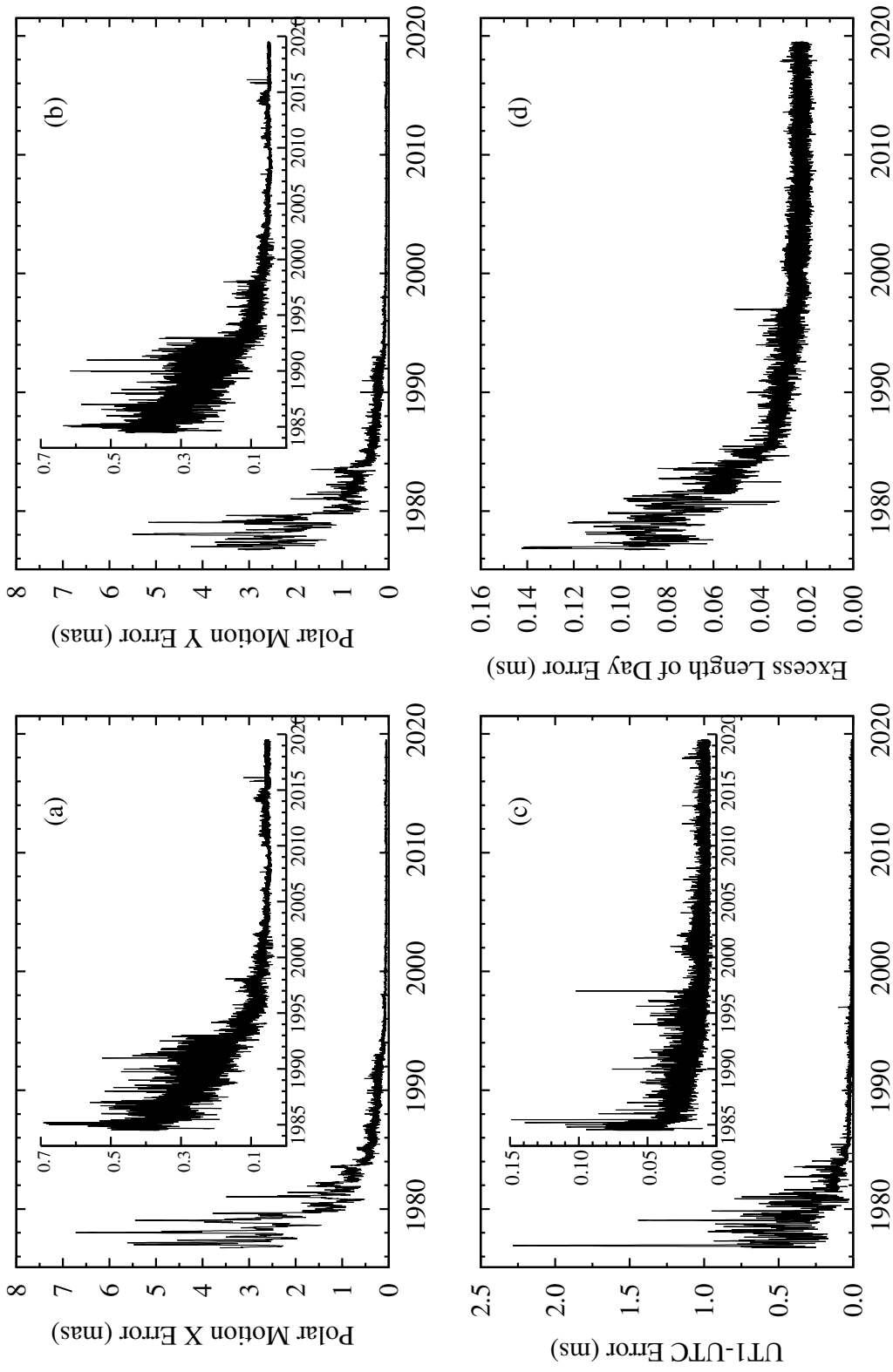# A Combined Earth Orientation Series: SPACE2018

Figure 2. Plots of the 1σ formal errors of the x-component of polar motion (2a), y-component of polar motion (2b), UT1–UTC (2c), and excess length-of-day (2d) as given by the combined Earth orientation series SPACE2018. The inserts within panels (2a), (2b), and (2c) show that component's post-1984 uncertainties on an expanded scale with the same units: milliarcseconds (mas) for polar motion, milliseconds (ms) for UT1–UTC.
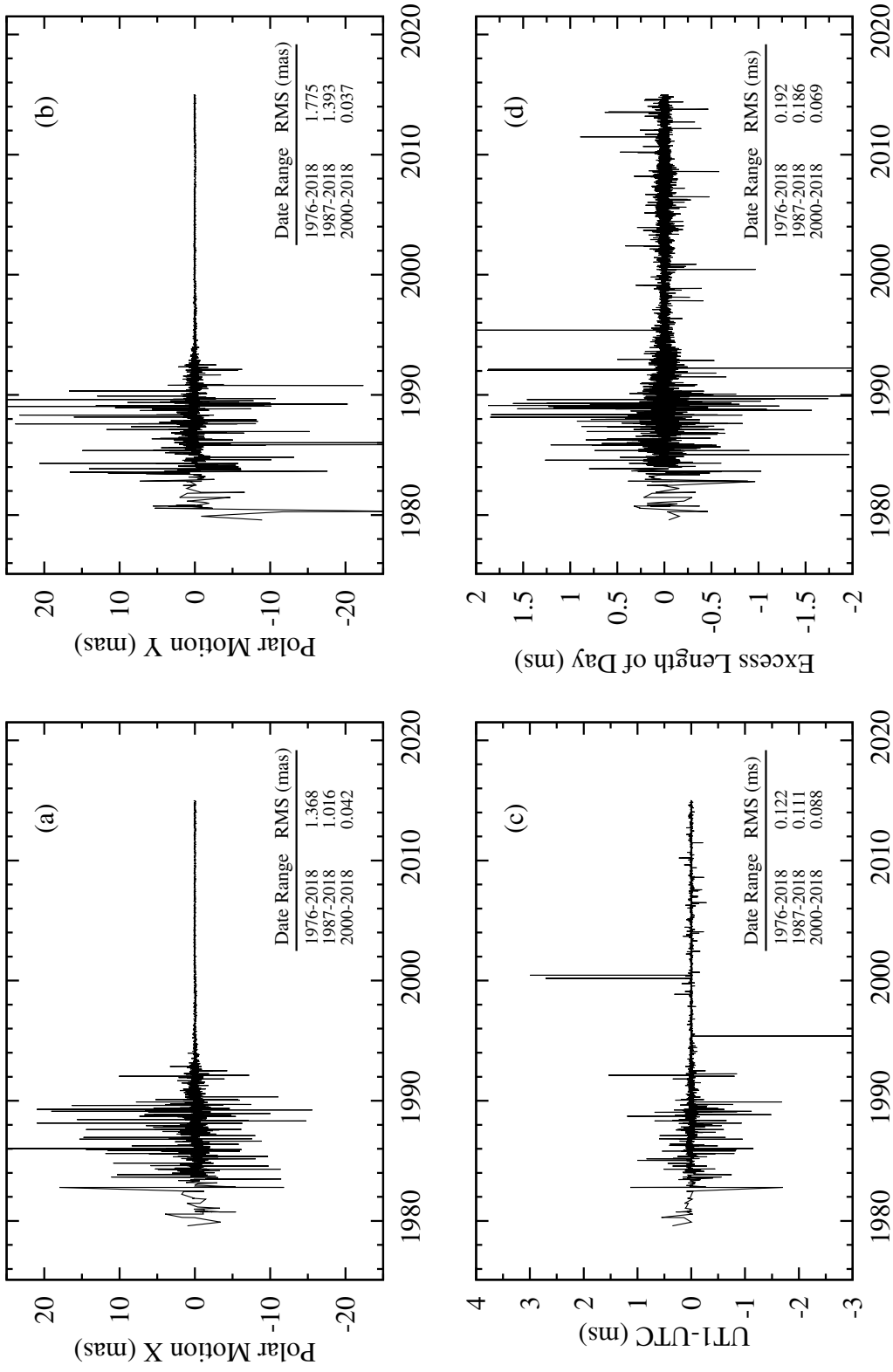
Difference of ITRF2014 with SPACE2018

Figure 3. Plots of the difference between the ITRF2014 Earth orientation parameters and SPACE2018 formed by subtracting the SPACE2018 values from those of the ITRF series. The difference between the x-component of polar motion is shown in (3a), the difference between the y-component is shown in (3b), the difference between UT1–UTC is shown in (3c), and the difference between the excess length-of-day is shown in (3d). Root Mean Square (rms) differences are tabulated as insets in each plot.
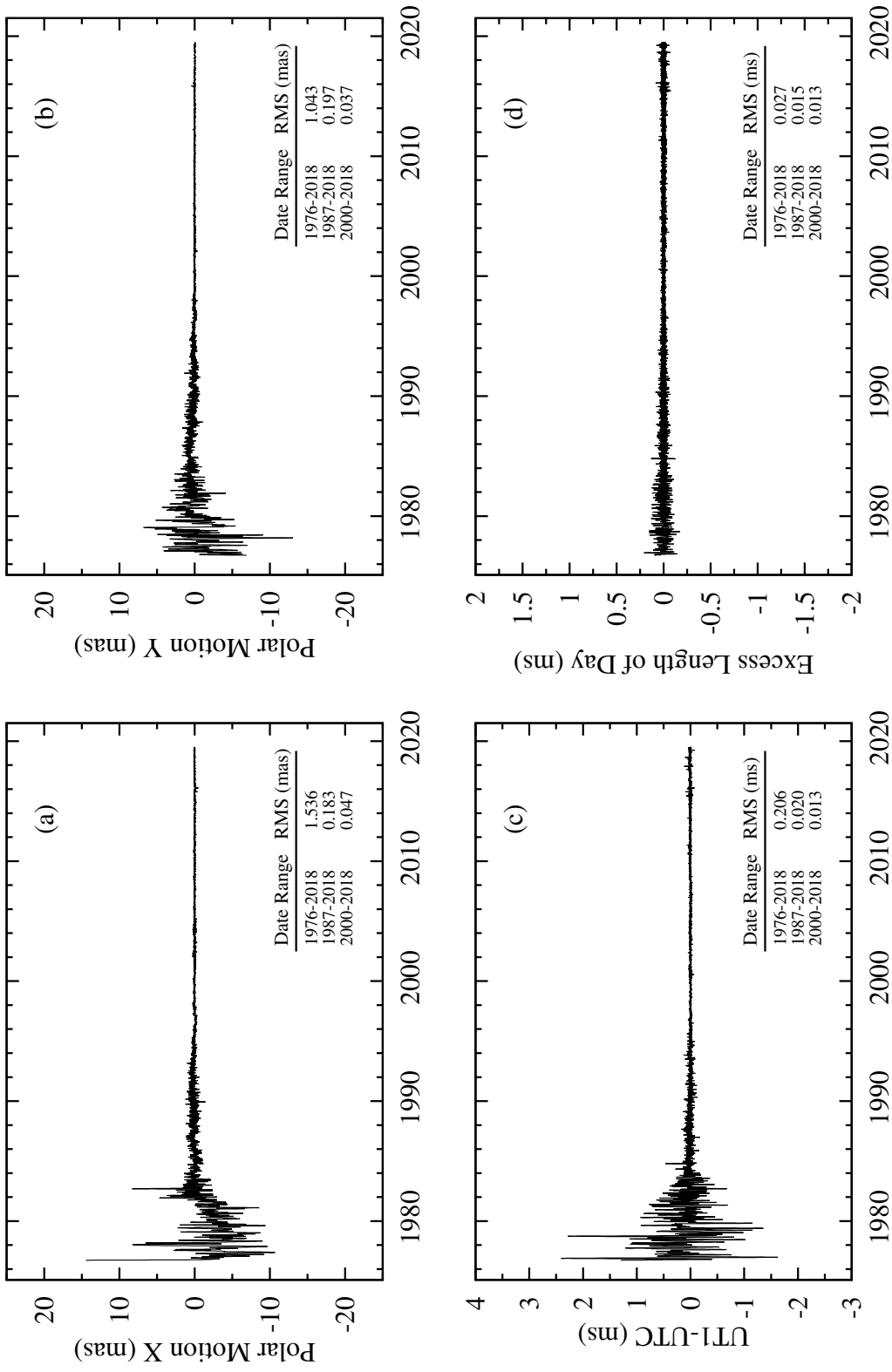
11

Figure 4. Plots of the difference between the IERS Bulletin A Earth orientation parameters and SPACE2018 formed by subtracting the SPACE2018 values from those of the Bulletin A series. The difference between the x-component of polar motion is shown in (3a), the difference between the y-component is shown in (3b), the difference between UT1–UTC is shown in (3c), and the difference between the excess length-of-day is shown in (3d). Root Mean Square (rms) differences are tabulated as insets in each plot.

12

COMB2018

COMB2018 extends SPACE2018 by additionally incorporating the optical astrometric polar motion and UT1 series that was determined at the Bureau International de l'Heure (BIH) from an analysis of time and latitude observations by Li (1985, also see Li & Feissel 1986). This BIH optical astrometric series consists of values and uncertainties for polar motion and UT1 that span from January 5.0, 1962, to December 31.0, 1981, at 5-day intervals. Also incorporated in COMB2018 are the McDonald Observatory LLR data that span from April 15, 1970 to September 13, 1976 that were not included in SPACE2018. These additional LLR points were adjusted in bias, rate, and uncertainty as per the McDonald Cluster in Table 3.

Data Preprocessing and Treatment of Tide-Induced Rotational Variations

The BIH optical astrometric series was preprocessed by removing leap seconds from the UT1 values and by correcting the UT1 values to be consistent with the extended definition of GST, as adopted by the IERS (IERS, 1997, p. I49). Rotational variations caused by solid Earth and ocean tides were also removed from the UT1 values. The same models that were used to remove the tidal effects from the series combined to form SPACE2018 were also used to remove them from the BIH series: namely, the Yoder et al. (1981) model for the solid Earth tides and the Kantha et al. (1998) model for the Mf, Mf′, and Mm ocean tides. However, since the BIH UT1 measurements represent an average value over a 5-day-long observation window, and since 5 days is a substantial fraction of the monthly and shorter-period tides, the amplitudes of these solid Earth and ocean tidal terms were attenuated prior to their removal from the BIH UT1 measurements. (See Gross 1996, p. 8735 and Gross et al. 1998, pp. 226–227 for further discussion about this point.)

Adjustments Made to BIH Series Prior to Combination

The preprocessed BIH optical astrometric series was combined with the space-geodetic series that comprise SPACE2018 after first:

1. Correcting the BIH series to have the same bias, rate, annual terms, and semiannual terms as SPACE2018;

2. Applying a constant multiplicative scale factor to the measurement uncertainties of the BIH series so that its residual, when differenced with SPACE2018, had a reduced chi-square of one; and

3. Deleting those data points, if any, for which residual values were greater than four times their adjusted uncertainties.

The above adjustments were determined in a multivariate approach as was done for the series combined to form SPACE2018. The procedure used to determine these bias-rate and seasonal term corrections, uncertainty scale factors, and outlying data points has been described before (Gross, 1996, pp. 8735–8738) and will not be repeated here. The annual and semiannual terms of the BIH series were adjusted in order to correct for systematic, seasonally varying effects that are known to be present in optical astrometric measurements. Since the values of both the BIH series and the SPACE2018 series are given at midnight, interpolation error (see Gross et al., 1998, pp. 223–225)

is automatically minimized when differencing these two series for the purpose of determining the adjustments to be made to the BIH series. Tables 4 and 5 give the resulting uncertainty scale factors and values and 1σ standard errors of the corrections to the bias, rate, annual terms, and semiannual terms thus determined for the BIH series. When determining these uncertainty scale factors and the corrections to the bias, rate, and seasonal terms, no outlying data points were detected.

Combined EOP Series: COMB2018

A Kalman filter was used to combine the BIH series with the adjusted space-geodetic series that comprise SPACE2018 after first applying to the BIH series the uncertainty scale factors and corrections to the bias, rate, annual, and semiannual terms that are given in Tables 4 and 5. The resulting combined Earth orientation series, COMB2018, consists of values (Figure 5) and 1σ standard errors (Figure 6) for polar motion, Universal Time, and their rates that span from January 20, 1962, to June 28, 2019, at daily intervals and is available in versions with epochs given at either midnight or noon. Leap seconds have been restored to UT1, and the effects of the solid Earth and ocean tides have been added back to the UT1 values using the same models for these effects that were originally used to remove them: namely, the Yoder et al. (1981) model for the solid Earth tides and the Kantha et al. (1998) model for the ocean tides. The full amplitude (i.e., no tidal terms attenuated) of the effects of the solid Earth and ocean tides at the epoch of the time tag were added back to the UT1 values. Semidiurnal and diurnal ocean tidal terms have not been added to and are, therefore, not included in the COMB2018 UT1 values.

Table 4. Adjustments to Bias, Rate, and Stated Uncertainty of Optical Astrometric Series[*]

Data Set	Bias, mas			Rate, mas/yr			Uncertainty Scale Factor		
	PMX	**PMY**	**UT1**	**PMX**	**PMY**	**UT1**	**PMX**	**PMY**	**UT1**
BIH	-1.9158 ± 0.8532	0.9802 ± 0.6965	-9.1312 ± 1.0587	0.8665 ± 0.5261	1.9993 ± 0.4264	5.6065 ± 0.6631	1.8136	1.6717	1.9265
ILS	-48.1214 ± 2.3494	-9.6190 ± 1.6336	-----	0.2504 ± 0.4801	0.7485 ± 0.3330	-----	2.1515	1.4696	-----

[*]Reference date for bias-rate adjustment of BIH series is 1980.0. Reference date for bias-rate adjustment of ILS series is 1970.0.

Table 5. Adjustment to Annual and Semiannual Terms of Optical Astrometric Series[*]

Data Set	Coeffecient of Sine Term, mas			Coefficient of Cosine Term, mas		
	PMX	**PMY**	**UT1**	**PMX**	**PMY**	**UT1**
BIH						
Annual	-4.8287 ± 1.0508	-8.8794 ± 0.8787	5.1814 ± 1.3603	-2.4437 ± 1.1219	9.4421 ± 0.9194	-0.4198 ± 1.4161
Semiannual	2.4160 ± 1.0729	-0.5648 ± 0.8936	-0.6844 ± 1.3836	1.1202 ± 1.0960	0.0962 ± 0.9006	1.8279 ± 1.3907
ILS						
Annual	-1.5691 ± 3.2772	6.7664 ± 2.2700	-----	8.4677 ± 3.3131	-10.6313 ± 2.2986	-----
Semiannual	0.3360 ± 3.2856	8.6915 ± 2.2770	-----	2.3611 ± 3.3017	1.0461 ± 2.2895	-----

[*]Reference date for adjustment of annual and semiannual terms of BIH series is 1980.0.
Reference date for adjustment of annual and semiannual terms of ILS series is 1970.0.

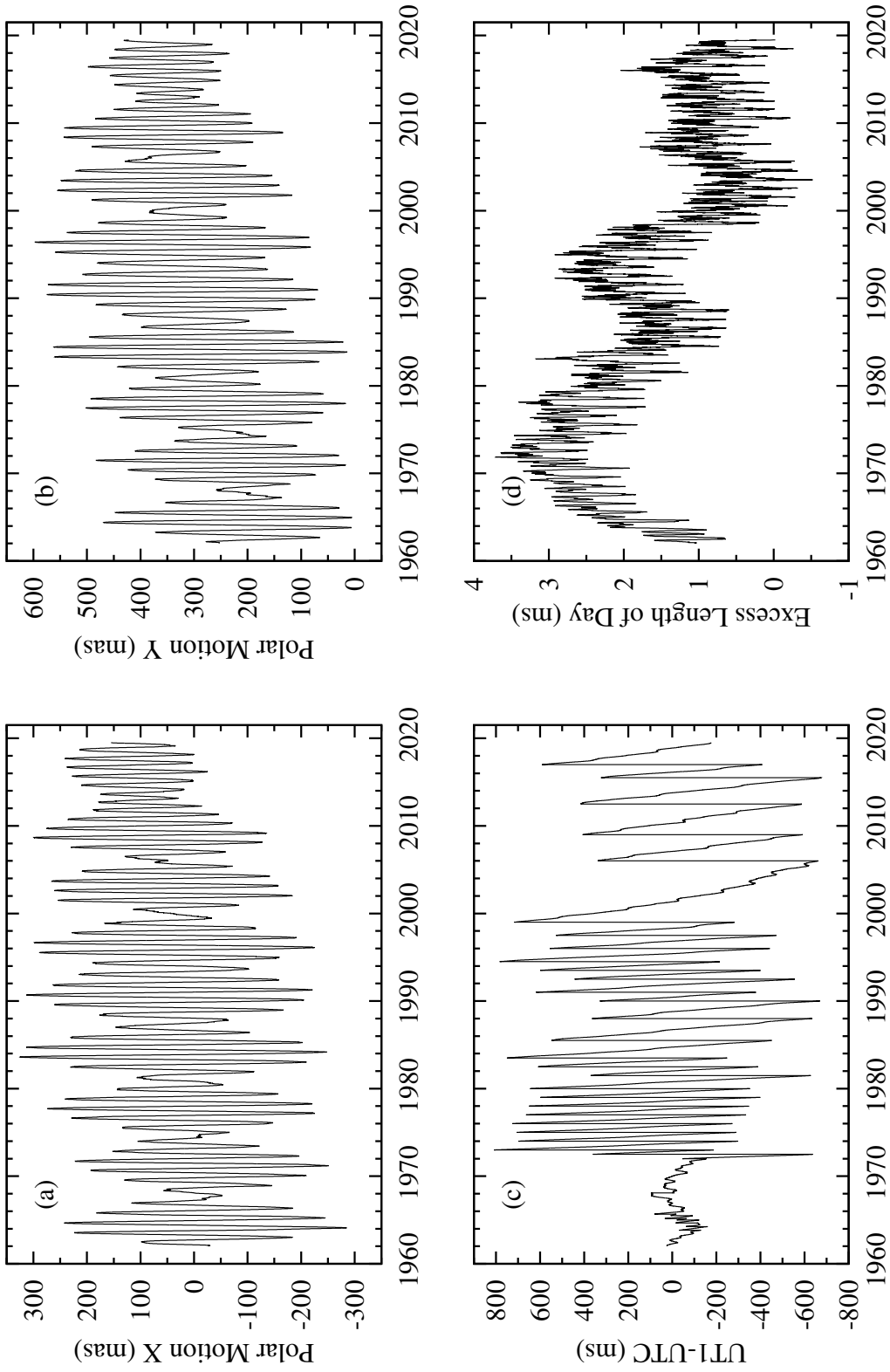# A Combined Earth Orientation Series: COMB2018

Figure 5. Plots of the x-component of polar motion (5a), y-component of polar motion (5b), UT1–UTC (5c), and excess length-of-day (5d) as given by the combined Earth orientation series, COMB2018. The discontinuous changes in the plot of UT1–UTC are caused by the presence of leap seconds. Prior to the introduction of leap seconds in 1972, Coordinated Universal Time (UTC) was adjusted by introducing step and rate changes designed to keep it close to UT1 (e.g., IERS, 1997, Table II-3), the effect of which is also readily apparent in (5c). Note that the UT1–UTC values displayed in (5c) include the tidal variations, whereas the excess length-of-day values shown in (5d) do not.
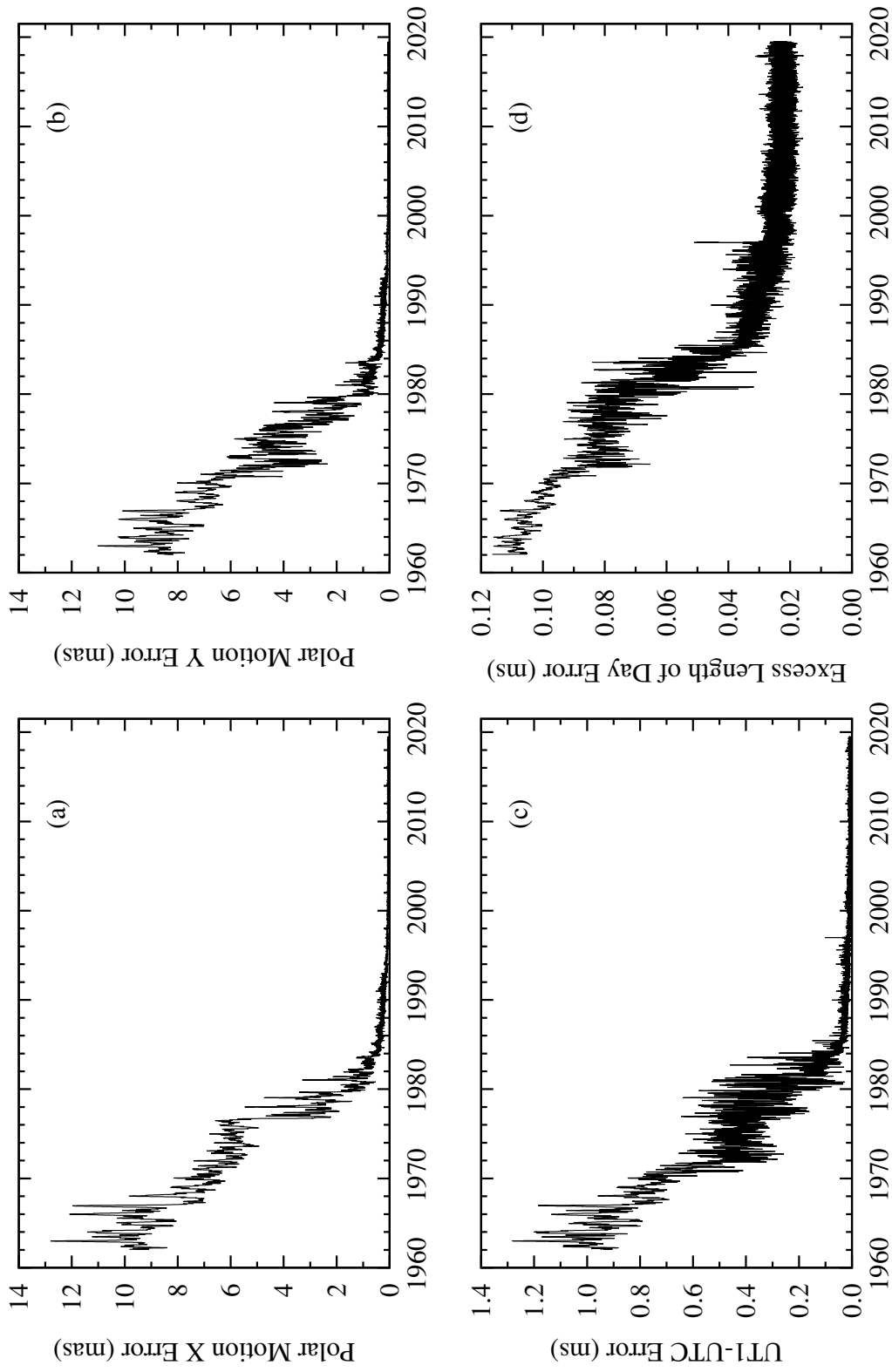
15

A Combined Earth Orientation Series: COMB2018

Figure 6. Plots of the 1σ formal errors of the x-component of polar motion (5a), y-component of polar motion (5b), UT1–UTC (5c), and excess length-of-day (5d) as given by the combined Earth orientation series COMB2018.

16

POLE2018

No optical astrometric observations taken at the stations of the International Latitude Service (ILS) were used when creating the BIH optical astrometric series used in COMB2018 (Li, 1985; Li & Feissel, 1986). The ILS polar motion measurements (Yumi & Yokoyama, 1980), which are based solely upon latitude observations made at the ILS stations are, therefore, independent of those comprising COMB2018 and have therefore been combined with them to form POLE2018. Being based solely upon latitude observations, the ILS series contains no UT1 measurements, but consists solely of polar motion measurements that span 1899.8–1979.0 at monthly intervals. Although no uncertainties are given with the individual polar motion values, the precision with which they have been determined is estimated to be 10–20 mas (Yumi & Yokoyama, 1980, p. 27). An initial uncertainty of 15 mas was, therefore, assigned to each of the ILS polar motion values. Since this assigned measurement uncertainty will be adjusted later, its initial value is arbitrary as long as it is not zero and serves merely as an a priori estimate to be used in the series adjustment procedure described below.

The ILS series was combined with COMB2018 to form POLE2018 after:

1. Correcting the ILS series to have the same bias, rate, annual terms, and semiannual terms as COMB2018;

2. Applying a constant multiplicative scale factor to the measurement uncertainties of the ILS series so that its residual, when differenced with COMB2018, had a reduced chi-square of one; and

3. Deleting those data points, if any, for which residual values were greater than four times their adjusted uncertainties.

These adjustments were also determined using a multivariate approach for fitting a bias, a rate, and these seasonal terms to the difference of the ILS series with COMB2018 during 1962.0 to 1979.0. The measurement uncertainties of the ILS polar motion values were adjusted by determining and applying a scale factor that made the residual of this fit have a reduced chi-square of one. During this procedure to determine uncertainty scale factors and bias, rate, and seasonal term corrections, no outlying ILS data points were deleted since no data points had residual values greater than four times their adjusted uncertainties. Tables 4 and 5 (in the COMB2018 section) also give the resulting uncertainty scale factors and values and 1σ standard errors of the corrections to the bias, rate, annual terms, and semiannual terms thus determined for the ILS series.

A Kalman filter was then used to combine the ILS series with the adjusted BIH and space-geodetic series that comprise COMB2018, after applying to the ILS series the uncertainty scale factors and corrections to the bias, rate, annual, and semiannual terms that are given in Tables 4 and 5. The resulting combined Earth orientation series, POLE2018, consists of values (Figure 7a and 7b) and 1σ standard errors (Figure 7c and 7d) for polar motion and its rate that span from January 20, 1900, to June 22, 2019, at 30.4375-day intervals.

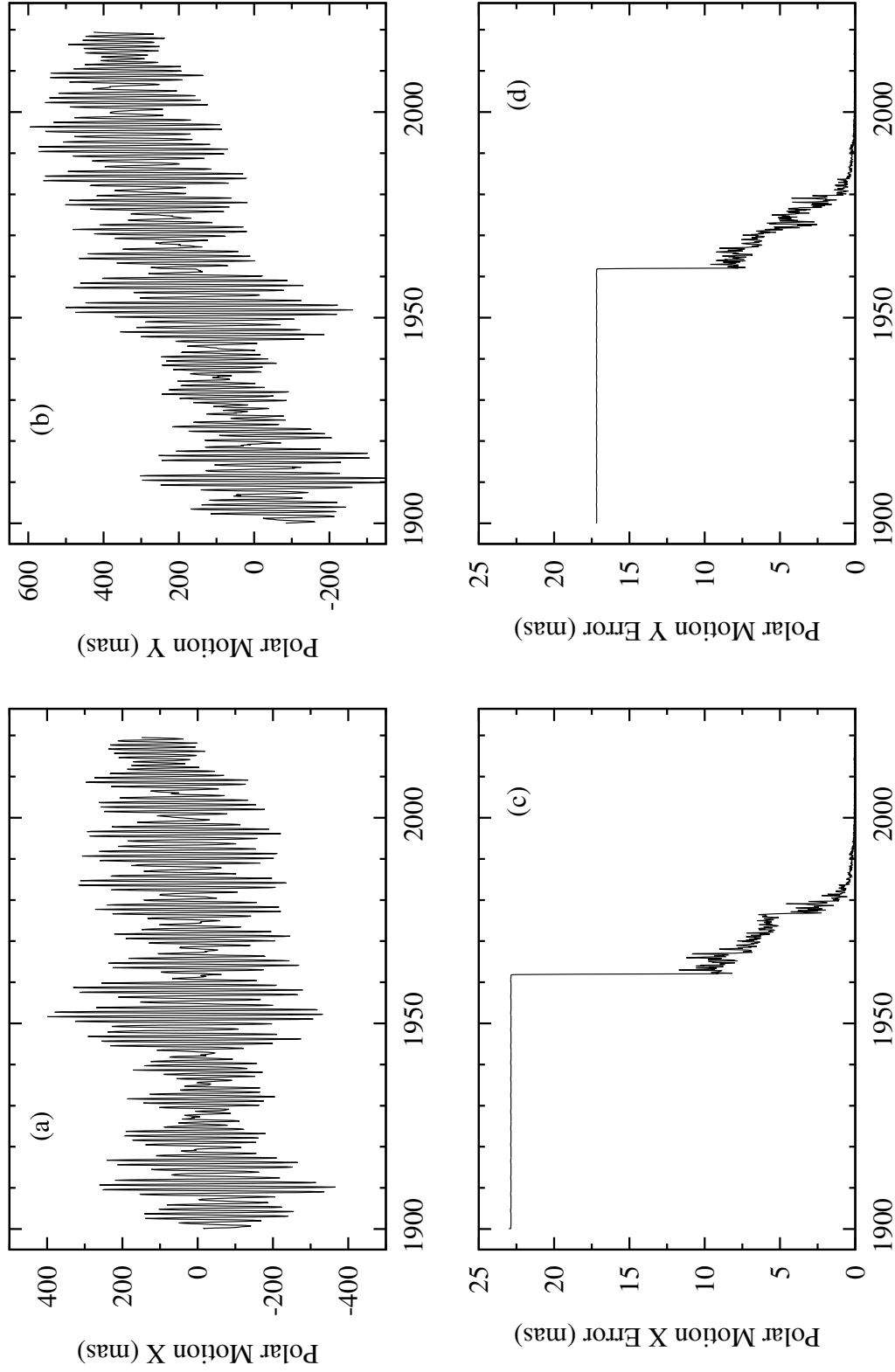# A Combined Earth Orientation Series: POLE2018

Figure 7. Plots of the x-component of polar motion (6a), the y-component of polar motion (6b), the 1σ formal errors of the x-component of polar motion (6c), and the 1σ formal errors of the y-component of polar motion (6d) as given by the combined polar motion series POLE2018.

18

DISCUSSION

The Kalman filter that was used here to combine Earth-orientation measurements contains a stochastic model of the process that is used to propagate the state vector and its associated state covariance matrix forward in time to the epoch of the next measurement. For polar motion excitation, the stochastic model includes a random-walk term with equal noise forcing both the x- and y-components of excitation and originally having a white-noise power spectral density of 246.4 mas^2/day (Morabito et al., 1988). This level of polar motion excitation process noise in the Kalman filter was increased to 739.2 mas^2/day in order to better match the observed spectrum of polar motion excitation. Increasing the excitation process noise reduces the level of smoothing applied to the polar motion components of the propagated state vector and increases the covariance associated with those components. Thus, the SPACE2018, COMB2018, and POLE2018 polar motion and polar-motion excitation values are not as heavily smoothed as were those of SPACE2003, COMB2003, POLE2003, and earlier combinations produced at JPL; and the uncertainties assigned to the SPACE2018, COMB2018, and POLE2018 polar motion and polar-motion excitation values are somewhat larger.

The LOD components of the IGS Final combined EOP(IGS) 95 P 02 and EOP (IGS) 00 P 03 series were incorporated into JPL's combinations starting with SPACE2007 and COMB2007. In general, GPS LOD estimates are contaminated by orbital artifacts that must be removed prior to combination with other LOD or UT1 measurements (Chin et al., 2009). When determining the IGS Final combined LOD series, however, the IGS applies constraints that have the effect of removing these orbital artifacts. Therefore the IGS Final combined LOD series was incorporated into the Kalman filter as a true LOD measurement for which uncertainties are assumed to be "white" (i.e., random, uncorrelated in time, and with a flat power spectral density). Including the daily IGS Final combined LOD series in JPL's combinations helps to compensate for less frequent UT1 measurements and was found to improve the agreement of JPL's combined LOD estimates with independent atmospheric and oceanic angular momentum values, especially at the highest frequencies.

Since a Kalman filter has been used to generate SPACE2018, COMB2018, and POLE2018, the resulting polar motion and UT1 values are smoothed to a degree that depends upon both the spacing between the measurements being combined (which determines how far the state vector and state covariance matrix must be propagated forward in time) and the uncertainties that have been assigned to the measurements. Since improvements to the observing systems, both in the hardware and software and in the number of systems, have led to increasingly precise determinations of the Earth's orientation, and since the time resolution of the measurements has generally increased in concert with the measurement precision, the degree of smoothing applied to the SPACE2018, COMB2018, and POLE2018 values is a function of time, with the earlier values being more heavily smoothed than the more recent values.

Daily EOP values are reported in SPACE2018 since the NOAA IRIS and GSFC NEOS Intensive UT1 values are given at daily intervals, as are the GPS and ILRSA combined SLR values (although gaps exist in each of these data sets). However, prior to the start of these data sets, the measurements combined to form SPACE2018 are given less frequently; therefore, the Kalman filter used to combine these measurements also interpolates them in order to produce a series of equally spaced values. In order to be consistent with SPACE2018, daily EOP values are also reported in COMB2018 even though the BIH optical astrometric series used in COMB2018 is given at 5-day intervals. Thus, SPACE2018, COMB2018, and POLE2018 are equally spaced series of smoothed, interpolated Earth-orientation parameters.

The combined Earth-orientation series SPACE2018, COMB2018, and POLE2018 are available from JPL's Geodynamics and Space Geodesy Group at:
`<https://keof.jpl.nasa.gov/combinations/2018>` and upon request from the authors: Todd.Ratcliff@jpl.nasa.gov or Richard.Gross@jpl.nasa.gov.

References

Altamimi, Z., P. Rebischung, L. Mètivier, and X. Collilieux. Complete EOP list file. ITRF website, 2016a. `ftp://itrf.ign.fr/pub/itrf/itrf2014/ITRF2014_EOP-F1.DAT`. Website accessed Sep. 22, 2017.

Altamimi, Z., P. Rebischung, L. Mètivier, and X. Collilieux. ITRF2014: A new release of the international terrestrial reference frame modeling nonlinear station motions. *Journal of Geophysical Research: Solid Earth*, 121(8):6109–6131, 2016b. ISSN 2169-9356. doi:10.1002/2016JB013098. `http://dx.doi.org/10.1002/2016JB013098`. 2016JB013098.

Chin, T. M., R. S. Gross, D. H. Boggs, and J. T. Ratcliff. Dynamical and observation models in the Kalman Earth orientation filter. In *The Interplanetary Network Progress Report*, Volume 42–176. Jet Propulsion Laboratory, California Institute of Technology, Pasadena, California, Feb. 2009. `http://ipnpr.jpl.nasa.gov/progress_report/42-176/176A.pdf`.

Eanes, R. J. and M. M. Watkins. Earth orientation and site coordinates from the Center for Space Research solution. In *1995 IERS Annual Report*, pages II8–II9. Obs. de Paris, Paris, 1996.

Eubanks, T. M., B. A. Archinal, F. J. Josties, and J. R. Ray. Earth orientation analysis from the U.S. Naval Observatory VLBI program. In *International VLBI Service for Geodesy and Astrometry 1999 Annual Report*, N. R. Vandenberg, ed., NASA/TP-1999-209243, pages 236–240. Greenbelt, Maryland, 1999.

Ferland, R. Original / new realization of ITRF97. IGS e-mail archive, Jet Propulsion Laboratory, California Institute of Technology, Oct. 19, 2000. `https://igscb.jpl.nasa.gov/pipermail/igsmail/2000/002973.html`.

Ferland, R. IGb00 - update. IGS e-mail archive, Jet Propulsion Laboratory, California Institute of Technology, Dec. 5, 2003. `https://igscb.jpl.nasa.gov/pipermail/igsmail/2003/004819.html`.

Ferland, R. Proposed IGS05 realization. IGS e-mail archive, Jet Propulsion Laboratory, California Institute of Technology, Oct. 19, 2006. `http://igscb.jpl.nasa.gov/pipermail/igsmail/2006/005518.html`.

Gordon, D., C. Ma, and D. MacMillan. GSFC VLBI analysis center annual report. In *International VLBI Service for Geodesy and Astrometry 1999 Annual Report*, N. R. Vandenberg, ed., NASA/TP-1999-209243, pages 203–206. 1999.

Gross, R. S. Combinations of Earth orientation measurements: SPACE94, COMB94, and POLE94. *J. Geophys. Res.*, 101:8729–8740, 1996.

Gross, R. S. Combinations of Earth orientation measurements: SPACE97, COMB97, and POLE97. *J. Geodesy*, 73:627–637, 2000.

Gross, R. S., T. M. Eubanks, J. A. Steppe, J. O. D. A. P. Freedman, and T. F. Runge. A Kalman filter-based approach to combining independent Earth orientation series. *J. Geodesy*, 72:215–235, 1998.

Heflin, M. B., Y. E. Bar-Sever, D. C. Jefferson, R. F. Meyer, B. J. Newport, Y. Vigue-Rodi, F. H. Webb, and J. F. Zumberge. JPL IGS Analysis Center Report, 2001–2003. In *IGS 2001-2002 Technical Reports*, K. Gowey, R. Neilan, and A. Moore, eds., JPL Publication 4-17, pages 65–70. Jet Propulsion Laboratory, California Institute of Technology, Pasadena, California, 2004.

Herring, T. A. Diurnal and semidiurnal variations in Earth rotation. In *Observations of Earth from Space*, Volume 13 of *Adv. Space Res.*, R. P. Singh, M. Feissel, B. D. Tapley, and C. K. Shum, eds., pages (11)281–(11)290. Pergamon, Oxford, 1993.

Herring, T. A. and D. Dong. Measurement of diurnal and semidiurnal rotational variations and tidal parameters of Earth. *J. Geophys. Res.*, 99:18051–18071, 1994.

IERS. *1996 IERS Annual Report*. Obs. de Paris, Paris, 1997.

IGS Analysis Center Coordinator. Chronology of IGS reference frame usage. IGS ACC website, 2012. `http://acc.igs.org/igs-frames.html`. Website accessed Sep. 3, 2017.

Kantha, L. H., J. S. Stewart, and S. D. Desai. Long-period lunar fortnightly and monthly ocean tides. *J. Geophys. Res.*, 103:12639–12647, 1998.

Kouba, J. and Y. Mireault. Analysis coordinator report. In *IGS 1996 Annual Report*, J. F. Zumberge, D. E. Fulton, and R. E. Neilan, eds., pages 55–100. Jet Propulsion Laboratory, California Institute of Technology, Pasadena, California, 1997.

Kouba, J., J. Ray, and M. Watkins. IGS reference frame realization. In *1998 IGS Analysis Center Workshop Proceedings*, pages 139–171. 1998.

Li, Z. Earth rotation from optical astrometry, 1962.0–1982.0. In *Bureau International de l'Heure Annual Report for 1984*, pages D31–D63. Paris, 1985.

Li, Z. and M. Feissel. Determination of the Earth rotation parameters from optical astrometry observations, 1962.0–1982.0. *Bull. Géod.*, 60:15–28, 1986.

Mireault, Y. and J. Kouba. IGS combinations of polar motion, length of day, and Universal Time. In *Towards an Integrated Global Geodetic Observing System (IGGOS)*, R. Rummel, H. Drewes, W. Bosch, and H. Hornik, eds., pages 154–157. Springer-Verlag, New York, 2000.

Morabito, D. D., T. M. Eubanks, and J. A. Steppe. Kalman filtering of Earth orientation changes. In *The Earth's Rotation and Reference Frames for Geodesy and Geodynamics*, A. K. Babcock, G. A. Wilkins, and D. Reidel, eds., pages 257–267. Springer, Dordrecht, Holland, 1988.

NASA/GSFC, VLBI Group. Very long baseline interferometry. NASA Goddard Space Flight Center VLBI Group website, Greenbelt, Maryland, 2018. `http://vlbi.gsfc.nasa.gov`. Website accessed Aug. 1, 2018.

Ratcliff, J. T. and R. S. Gross. *Combinations of Earth Orientation Measurements: SPACE2017, COMB2017, and POLE2017*. JPL Publication 18-5. Jet Propulsion Laboratory, California Institute of Technology, Pasadena, California, 2018.

Ray, J. R., M. D. Abell, W. E. Carter, W. H. Dillinger, and M. L. Morrison. NOAA Earth orientation and reference frame results derived from VLBI observations: Final report. In *Earth Orientation, Reference Frames, and Atmospheric Excitation Functions Submitted for the 1994 IERS Annual Report*, P. Charlot, ed., IERS Technical Note 19, pages R33–R38. Paris, 1995.

Rebischung, P. IGb08: an update on IGS08, IGSMAIL-6663. IGS e-mail archive, Jet Propulsion Laboratory, California Institute of Technology, Pasadena, California, Sep. 24, 2012. `http:// igscb.jpl.nasa.gov/pipermail/igsmail/2012/007853.html`.

Rebischung, P. Upcoming switch to IGS14/igs14.atx, IGSMAIL-7399. IGS e-mail archive, Jet Propulsion Laboratory, California Institute of Technology, Pasadena, California, Dec. 21, 2016. `https://igscb.jpl.nasa.gov/pipermail/igsmail/1999/002507.html`.

Rebischung, P. and B. Garayt. Recent results from the IGS terrestrial frame combinations. In *Reference Frames for Applications in Geosciences*, Volume 138, A. Zuheir and X. Collilieux, eds., pages 69–74. Springer, Berlin, 2013.

Rebischung, P., J. R. J. Griffiths, R. Schmid, X. Collileux, and B. Garayt. IGS08: The IGS realization of ITRF2008. *GPS Solutions*, 16:483–494, 2012. doi:10.1007/s10291-011-0248-2.

Rebischung, P., R. Schmid, and J. Ray. Upcoming switch to IGS08/igs08.atx, IGSMAIL-6354. IGS e-mail archive, Jet Propulsion Laboratory, California Institute of Technology, Pasadena, California, Mar. 7, 2011. `http://igscb.jpl.nasa.gov/pipermail/igsmail/2011/ 006346.html`.

Sciaretta, C., V. Luceri, E. C. Pavlis, and G. Bianco. The ILRS EOP time series. *Artificial Satellites*, 45(2):41–48, 2010. doi:10.2478/v10018-010-0004-9.

Springer, T. ITRF96/97 IGS product changes. IGS e-mail archive, Jet Propulsion Laboratory, California Institute of Technology, Pasadena, California, Aug. 20, 1999. `http://igscb.jpl. nasa.gov/pipermail/igsmail/2012/007853.html`.

Stamatakos, N., M. Davis, N. Summate, M. S. Carter, and C. Hackman. Rapid service/prediction centre. In *IERS Annual Report 2014*, W. R. Dick and D. Thaller, eds., pages 70–88. Bundesamts für Kartographie und Geodäsie, Frankfurt am Main, Germany, 2015.

Steppe, J. A., S. H. Oliveau, and O. J. Sovers. Earth rotation parameters from DSN VLBI: 1997. In *1996 IERS Annual Report*, page II24. Obs. de Paris, Paris, 1997.

Weber, R. Towards ITRF2000. IGS e-mail archive, Jet Propulsion Laboratory, California Institute of Technology, Nov. 21, 2001. `https://igscb.jpl.nasa.gov/pipermail/igsmail/ 2001/003679.html`.

Williams, J. G., D. H. Boggs, S. G. Turyshev, J. O. Dickey, and J. T. Ratcliff. Report of the Jet Propulsion Laboratory (JPL) lunar associate analysis center. In *International Laser Ranging Service 2009–2010 Report*, C. Noll and M. Pearlman, eds., NASA Tech. Pub. 2013-217507, pages 11.58–11.59. Greenbelt, Maryland, 2012.

Yagudina, E. I., D. A. Pavlov, V. N. Tryapitsyn, and V. V. Rumyantsev. Processing and analysis of lunar laser ranging observations in crimea in 1974-1984. presented at the 2018 International Workshop on Laser Ranging, 2018.

Yoder, C. F., J. G. Williams, and M. E. Parke. Tidal variations of Earth rotation. *J. Geophys. Res.*, 86:881–891, 1981.

Yumi, S. and K. Yokoyama. *Results of the International Latitude Service in a Homogeneous System, 1899.9-1979.0*. The Central Bureau of the International Polar Motion Service and the International Latitude Observatory of Mizusawa, Mizusawa, Japan, 1980.

Acronyms and Terms

ASI   Agenzia Spaziale Italiana

BIH   Bureau International de l'Heure

CGS   Centro di Geodesia Spaziale
CODE   Center for Orbit Determination in Europe
COMB   extends the SPACE series by additionally incorporating BIH optical astrometric measurements of polar motion and UT1

DSN   Deep Space Network

EOP   Earth orientation parameter

G3   IVS station code for 85-3 antenna at NRAO Green Bank, WV
Gc   IVS station code for Gilmore Creek, Fairbanks, AK
GNSS   Global Navigation Satellite System
GPS   Global Positioning System
GSFC   Goddard Space Flight Center
GST   Greenwich Sidereal Time

Hr   IVS station code for HRAS
HRAS   Harvard Radio Astronomy Station at Ft. Davis, TX

ID   Identification
IERS   International Earth Rotation and Reference Systems Service
IGN   Institut National de l'Information Géographique et Forestière
IGS   International Global Navigation Satellite Systems (GNSS) Service
ILRS   International Laser Ranging Service
ILRSA   ILRS Primary Combination Solution
ILS   International Latitude Service
IRIS   International Radio Interferometric Surveying
ITRF   International Terrestrial Reference Frame
IVS   International VLBI Service for Geodesy & Astrometry

JPL   Jet Propulsion Laboratory

Kk   IVS station code for Kokee Park, Kauai, HI
Ku   IVS station code for 9-m antenna at Kokee Park, Kauai, HI

LAGEOS Laser Geodynamics Satellites
LLR   lunar laser ranging
LOD   length-of-day

mas	milliarcsecond
Mo	IVS station code for 12-m antenna at Goldstone, CA
ms	millisecond
NASA	National Aeronautics and Space Administration
NEOS	National Earth Orientation Service
NOAA	National Oceanic and Atmospheric Administration
NRAO	National Radio Astronomy Observatory
NRCan	Natural Resources Canada
Ny	IVS station code for Ny Alesund, Svalbard, Norway
OCA	Observatoire de la Côte d'Azur
PMX	polar motion X
PMY	polar motion Y
POLE	extends the COMB series by additionally incorporating ILS optical astrometric measurements of polar motion
Ri	IVS station code for Richmond, FL
rms	root mean square
SINEX	Solution Independent Exchange
SLR	satellite laser ranging
SPACE	a combination of independent space-geodetic measurements of Earth's orientation
Sv	IVS station code for Svetloe, Russia
T	transverse component of Earth orientation from single-baseline VLBI
Ts	IVS station code for 32-m antenna at Tsukuba, Japan
USNO	United States Naval Observatory
UT	Universal Time
UT0	Universal Time as determined at a particular observatory
UT1	The principle form of Universal Time; mean solar time at $0°$ longitude obtained by correcting UT0 for observatory location and polar motion.
UTC	Coordinated Universal Time
UTCSR	University of Texas Center for Space Research
V	vertical component of Earth orientation from single-baseline VLBI
VLBI	very long baseline interferometry
VOL	variation of latitude
Wf	IVS station code for Westford, MA
Wz	IVS station code for Wettzell, Germany